

Hybrid Particle-Field Coarse-Grained Models for Biological Phospholipids

Antonio De Nicola,^{†,‡} Ying Zhao,[†] Toshihiro Kawakatsu,[§] Danilo Roccatano,^{||} and Giuseppe Milano^{†,‡,*}

[†]Dipartimento di Chimica e Biologia, Università di Salerno, I-84084 via Ponte don Melillo Fisciano (SA), Italy

[‡]IMAST Scarl-Technological District in Polymer and Composite Engineering, P.le Fermi 1, 80055 Portici (NA), Italy

[§]Department of Physics, Tohoku University, Aoba, Aramaki, Aoba-ku, Sendai 980-8578, Japan

^{||}Jacobs University Bremen, Campus Ring 1, D-28759 Bremen, Germany

 Supporting Information

ABSTRACT: In the framework of a recently developed scheme for a hybrid particle-field simulation technique where self-consistent field theory (SCF) and molecular dynamics (MD) are combined [*J. Chem. Phys.* **2009**, *130*, 214106], specific coarse-grained models for phospholipids and water have been developed. We optimized the model parameters, which are necessary in evaluating the interactions between the particles and the density fields, so that the coarse-grained model can reproduce the structural properties of the reference particle–particle simulations. The development of these specific coarse-grained models suitable for hybrid particle-field simulations opens the way toward simulations of large-scale systems employing models with chemical specificity, especially for biological systems.

1. INTRODUCTION

Phospholipids are an important class of biomolecules. Their amphiphilic nature allows them, when they are dissolved in water, to self-assemble into a lipid bilayer with lipid tails shielded from water and polar head groups exposed to the polar environment. In living organism, lipid bilayers form cellular membranes. Biological membranes are complex structures, and despite the considerable amount of information accumulated, experimental methods able to follow their dynamics with details at the atomic level are not yet available.^{1–5} For these reasons, lipid bilayers have attracted the interest of the computational biophysics community, and atomistic molecular dynamics (MD) simulations of these systems have been performed for a long time.^{6–10} However, these simulations are still computationally very expensive to study processes occurring on the mesoscopic time ($>\mu\text{s}$) and length scales ($>100 \text{ nm}$).¹¹ Therefore, to overcome this problem, alternative computational methods aiming to bridge the time and length scales involved in the relevant phenomena are constantly proposed. In the past few years, coarse-grained (CG) simulations became a very popular method for studying these systems. The CG approach involves the reduction of degrees of freedom in the atomic model of the simulated system by combining several atoms to a single particle (“effective bead”). CG methods have been successfully applied to several problems involving polymers,¹² biomolecules,² and more in general soft matter.¹³

For phospholipids, different types of CG models have been developed. For a detailed overview, the reader should refer to a recent review of Muller et al.¹⁴ Sintes and Baumgärtner^{15,16} developed a coarse-grained model for lipid bilayers where the solvent is implicitly taken into account. Later, Lenz and Schmid developed this implicit-solvent model to pure lipid bilayers composed of saturated lipids.¹⁷ On the other hand, Goetz and Lipowsky introduced an explicit-solvent CG model for lipid

membranes where a binary Lennard-Jones fluid for the solvent and a short chain of beads for the amphiphilic molecules are used.¹⁸

The degree of coarse-graining of a simulated system is related to the type of process that one wants to investigate. Minimalist CG models (e.g., having a very low discrimination of the chemical details of the molecule) can be successfully applied to study self-assembly phenomena involving many molecules when the structure and dynamics on atomistic length scales can be considered irrelevant for the process, and systems can be conveniently described by only a small number of key properties, e.g., the amphiphilic nature of the molecule. Usually for membrane systems, a clear separation in length, time, and energy scales assumed by this approach is often missing, and the chemical specificity of the models have to be taken into account. Furthermore, these simple models can fail to reproduce more complex phenomena involving specific interactions of membrane with other molecular systems (e.g. proteins, polymers). In these cases, the generic nature of the minimal coarse-grain models limits their application.

To possibly avoid these problems, more specific CG models can be developed. These CG models usually employ several different types of beads (not just hydrophobic and hydrophilic). A successful and very widely explored example of this approach is the MARTINI CG model developed by Marrink and co-workers.¹⁹ In the MARTINI force field, the phospholipids are described by beads having different Lennard-Jones-type interaction parameters that can smoothly modulate their hydrophobic/hydrophilic character. In addition, water molecules are treated explicitly with a coarse-grained reduction scheme of four molecules to one.

Received: February 23, 2011

Published: August 03, 2011

Despite, its simplicity, the MARTINI force field is able to reproduce with surprisingly good accuracy the properties of the self-assembly of lipid bilayers.^{8,20,21} This model has been successfully extended to proteins.²²

On the other hand, different computational approaches based on field representations have been proposed to model soft matter systems. In particular, in the framework of the self-consistent field (SCF) theory, the model systems are not represented by particles but by density fields, and the mutual interactions between segments are decoupled and replaced by an interaction between the segments and static external fields.²³ In the SCF theories, these external fields depend on the statistical average of the spatially inhomogeneous density distributions of segments of independent molecules which are interacting only with these fields. Such external fields and the particle density distributions have to be determined self-consistently. Numerous applications to block copolymers,^{24–28} proteins,²⁹ polymer composites,³⁰ and colloidal particles^{31,32} have demonstrated that the SCF theory is a useful and powerful method.

Several models have been reported in the literature to study mixtures of phospholipids and water using a field-based approach. Marcelja proposed the first field model. In this model, the head groups of the lipid molecules are modeled as a boundary to which the tails of the lipid molecules are anchored. The intramolecular degrees of freedom are sampled using the rotational isomeric state (RIS) model, where the segments interact through an anisotropic aligning potential.³³ The inequivalence of tail, head, and solvent segments allows the modeling of bilayers as preassembled structures, and it does not allow the study of self-assembly. Later, a fully self-consistent framework that is capable of describing stable, tensionless, self-assembled bilayers has been proposed. Both random-chain and the RIS-chain models result in membranes with qualitatively similar segment distributions and with similar thermodynamic properties.³⁴ Quantitatively, however, this approach underestimates the experimentally measured membrane thickness by about 50%.¹⁴ More recently, molecular-level SCF theories that are able to treat phospholipids have been proposed.³⁵ The main point of these SCF techniques is to split up the calculation of multibody interactions into two procedures: i.e., to find the ensemble averaged conformation distribution and to find the segment potentials based on the segment distribution. For these purposes, differential equations have to be solved numerically using lattice approximations, and a discrete set of coordinates onto which segments can be placed has to be defined. Layers are defined imposing reflecting boundary conditions to mimic a multilamellar system. Parameters are defined so that the results of the MD simulations match those of the SCF simulations.³⁵ Müller and Schick³⁶ proposed an alternative approach developing an off-lattice representation of the field theory and obtained the single-chain partition function via a partial enumeration³⁷ over a large set of molecular conformations of a lipid chain with the RIS statistics. As the partition function of a single lipid in an external field cannot be obtained analytically for a realistic molecular architecture, one has to approximate the probability distributions of the conformations of noninteracting lipid molecules by a representative sample of single lipid conformations.

More recently, Müller and Smith³⁸ introduced a hybrid approach in the framework of SCF theory by combining it with a Monte Carlo simulation of a coarse-grained model of polymer chains to study phase separation in binary polymer mixtures. This approach has been widely and successfully applied by Müller and

co-workers to coarse-grained models of diblock copolymer thin films³⁹ and polymer nanocomposites.⁴⁰ One of the advantages of this hybrid approach is the lack of any limitation in treating complex molecular architectures and/or intramolecular interactions. With these precedents, very recently, a hybrid particle-field approach, where the molecular dynamics (MD) method is combined with SCF description (MD-SCF), was proposed, and an implementation suitable for the treatment of atomistic force fields and/or specific coarse-grained models has been reported.^{41,42}

Particle-based CG models like MARTINI are still computationally expensive compared to SCF approaches. In the following, we will refer to these models as particle–particle (PP) models. On the other hand, SCF approaches ensure accessibility to definitely larger length and time scales but at the cost of very low chemical specificity. The idea behind the combined MD-SCF method is to obtain a strategy, as far as will be possible, having the main advantages and avoiding the main disadvantages of both techniques.

In this paper, we report the development of coarse-grained specific models for biologically relevant phospholipids that are suitable for the hybrid MD-SCF techniques. In the following, we will refer to these models as particle-field (PF) models.

The paper is organized as follows: In section 2, the basis of SCF theory, which is useful for the reader to understand in regard to the present investigation, a brief description of the computational scheme for hybrid particle-field MD-SCF simulations, and simulation details are reported. In section 3, the description of the models and the strategy of the parametrization are reported. In section 4, particle-field MD-SCF simulation results of lipid bilayers are reported in comparison with classical MD simulations using the MARTINI force field, where the latter simulations are hereafter called PP simulations.

2. COMPUTATIONAL METHOD

2.1. MD-SCF Theory and Implementation. In this section, a brief exposition of the recently developed hybrid PF MD-SCF simulation scheme is reported. This section is intended to quickly guide the reader to get the basis of the methodology and to understand the framework of the present investigation. In order to obtain this approach in more detail, the reader should refer to ref 41, where the complete derivation and the implementation are described, and to ref 23 for a general review of SCF methods.

The main feature of the hybrid PF MD-SCF approach is that the evaluation of the nonbonded force and its potential between atoms of different molecules, i.e., the most computationally expensive part of MD simulations, is replaced by an evaluation of the external potential that is dependent on the local density at position \mathbf{r} . According to the spirit of SCF theory, a many-body problem like molecular motion in systems composed of many molecules is reduced to a problem of deriving the partition function of a single molecule in an external potential $V(\mathbf{r})$. Then, nonbonded force between atoms of different molecules can be obtained from a suitable expression of the potential $V(\mathbf{r})$ and its derivatives.

In the framework of SCF theory, a molecule is regarded as interacting with the surrounding molecules not directly but through a mean field. On the basis of this picture, the Hamiltonian of a system that is composed of M molecules can be split into two parts $\hat{H}(\Gamma) = \hat{H}_0(\Gamma) + \hat{W}(\Gamma)$, where Γ specifies a point in the phase space, which is used as shorthand for a set of positions of all

atoms in the system. Here and also in the following, the hat symbol indicates that the associated physical quantity is a function of the microscopic states described by the phase space Γ .

$\hat{H}_0(\Gamma)$ is the Hamiltonian of a reference ideal system composed of noninteracting chains but with all the intramolecular interaction terms (bond, angle, and nonbonded interactions) that are taken into account in the standard MD simulations. The term $\hat{W}(\Gamma)$ is the deviation from the reference system which is induced by the intermolecular nonbonded interactions.

Assuming the canonical (*NVT*) ensemble, the partition function of this system is given by

$$Z = \frac{1}{M!} \int d\Gamma \exp\{-\beta[\hat{H}_0(\Gamma) + \hat{W}(\Gamma)]\} \quad (1)$$

where $\beta = 1/(k_B T)$.

From microscopic point of view, the density distribution of atoms can be defined as a sum of δ functions centered at the center of mass of each particle as

$$\hat{\phi}(\mathbf{r}; \Gamma) = \sum_{p=1}^M \sum_{i=0}^{S(p)} \delta(\mathbf{r} - \mathbf{r}_i^{(p)}) \quad (2)$$

where M is the total number of molecules in the system, $S(p)$ is the number of particles contained in p th molecule, and $\mathbf{r}_i^{(p)}$ is the position of the i th particle in p th molecule. Several assumptions are introduced to calculate the interaction term $\hat{W}(\Gamma)$. First of all, we assume that $\hat{W}(\Gamma)$ depends on Γ only through the particle density $\hat{\phi}(\mathbf{r}; \Gamma)$ as

$$\hat{W}(\Gamma) = W[\hat{\phi}(\mathbf{r}; \Gamma)] \quad (3)$$

where $W[\hat{\phi}(\mathbf{r}; \Gamma)]$ means that W is a functional of $\hat{\phi}(\mathbf{r}; \Gamma)$. Using an identity $f[\hat{\phi}(\Gamma)] = \int D\{\varphi(\mathbf{r})\} \delta[\varphi(\mathbf{r}) - \hat{\phi}(\Gamma)] f[\varphi(\mathbf{r})]$ where $\delta[\varphi(\mathbf{r})]$ is the δ functional, the partition function in eq 1 can be rewritten as

$$Z = \frac{1}{M!} \int D\{\varphi(\mathbf{r})\} \int D\{w(\mathbf{r})\} \exp \left\{ -\beta \left[-\frac{M}{\beta} \ln z + W[\varphi(\mathbf{r})] - \int V(\mathbf{r}) \varphi(\mathbf{r}) d\mathbf{r} \right] \right\} \quad (4)$$

In this expression, z is the single molecule partition function, $w(\mathbf{r})$ is a conjugate field of $\varphi(\mathbf{r})$ which appeared in the Fourier representation of the δ functional, and $V(\mathbf{r})$ is the external potential that is related to $w(\mathbf{r})$ as $V(\mathbf{r}) = (i/\beta)w(\mathbf{r})$.

For evaluating this partition function approximately, the integrals over $\varphi(\mathbf{r})$ and $w(\mathbf{r})$ in eq 4 are replaced with a Gaussian integral around the most probable state that minimizes the argument of the exponential function on the right side of eq 4 (so-called saddle point approximation).

The minimization conditions in the form of functional derivatives result in

$$\begin{cases} V(\mathbf{r}) = \frac{\delta W[\phi(\mathbf{r})]}{\delta \phi(\mathbf{r})} \\ \varphi(\mathbf{r}) = -\frac{M}{\beta z} \frac{\delta z}{\delta V(\mathbf{r})} = \langle \hat{\phi}(\mathbf{r}; \Gamma) \rangle = \phi(\mathbf{r}) \end{cases} \quad (5)$$

where $\phi(\mathbf{r})$ is the coarse-grained density at position \mathbf{r} .

In terms of eq 5, it is possible to acquire an expression for a density-dependent external potential acting on each segment.

Next, we assume that the density dependent interaction potential W , where each component species is specified by the index K , takes the following form:

$$W[\{\phi_K(\mathbf{r})\}] = \int d\mathbf{r} \left(\frac{k_B T}{2} \sum_{KK'} \chi_{KK'} \phi_K(\mathbf{r}) \phi_{K'}(\mathbf{r}) + \frac{1}{2\kappa} (\sum_K \phi_K(\mathbf{r}) - \phi_0)^2 \right) \quad (6)$$

where $\phi_K(\mathbf{r})$ is the coarse-grained density of the species K at position \mathbf{r} and $\chi_{KK'}$ represents the mean field parameters for the interaction of a particle of type K with the density fields due to particles of type K' . The second term of the integrand on the right-hand side of eq 6 is the relaxed incompressibility condition. κ is the compressibility that is assumed to be sufficiently small, and ϕ_0 is the total number density of segments (we assume that volume for all segments is the same). Then, the corresponding mean field potential is given by

$$V_K(\mathbf{r}) = \frac{\delta W[\{\phi_K(\mathbf{r})\}]}{\delta \phi_K(\mathbf{r})} = k_B T \sum_{K'} \chi_{KK'} \phi_{K'}(\mathbf{r}) + \frac{1}{\kappa} (\sum_K \phi_K(\mathbf{r}) - \phi_0) \quad (7)$$

Taking the case of a mixture of two components A and B as an example, the mean field potential acting on a particle of type A at position r is given by

$$V_A(\mathbf{r}) = k_B T [\chi_{AA} \phi_A(\mathbf{r}) + \chi_{AB} \phi_B(\mathbf{r})] + \frac{1}{\kappa} [\phi_A(\mathbf{r}) + \phi_B(\mathbf{r}) - \phi_0] \quad (8)$$

Thus, the force acting on the particle A at position \mathbf{r} imposed by the interaction with the density field is

$$\begin{aligned} F_A(\mathbf{r}) &= -\frac{\partial V_A(\mathbf{r})}{\partial \mathbf{r}} \\ &= -k_B T \left(\chi_{AA} \frac{\partial \phi_A(\mathbf{r})}{\partial \mathbf{r}} + \chi_{AB} \frac{\partial \phi_B(\mathbf{r})}{\partial \mathbf{r}} \right) \\ &\quad - \frac{1}{\kappa} \left(\frac{\partial \phi_A(\mathbf{r})}{\partial \mathbf{r}} + \frac{\partial \phi_B(\mathbf{r})}{\partial \mathbf{r}} \right) \end{aligned} \quad (9)$$

The main advantage of the hybrid MD-SCF scheme is that the most computationally expensive part of the MD simulations, i.e., the evaluation of the nonbonded force between atoms of different molecules, is replaced by the evaluation of forces between single molecules with an external potential. In order to connect particle and field models, for the proposed hybrid MD-SCF scheme, it is necessary to obtain a smooth coarse-grained density function directly from the particle positions Γ . Let us denote this procedure as

$$\bar{S}\{\hat{\phi}(\mathbf{r}; \Gamma)\} = \phi(\mathbf{r}) \quad (10)$$

where \bar{S} is a symbolic name of the mapping from the particle positions to the coarse-grained density. In order to obtain a smooth spatial density from particle positions, the simulation box is divided into several cells. In particular, particles are sorted and, according to their positions, assigned to $n_{cell} = n_x n_y n_z$ (where n_x , n_y , and n_z are the number of cells in the x , y , and z directions, respectively). Furthermore, according to the position of each particle inside a cell, a fraction of it will be assigned to each vertex of the cell. In Chart 1, a simple two-dimensional case is used to explain the procedure. In the same chart, the structure of a phospholipid and the corresponding density field are schematized.

As shown in Chart 1B, the fraction of a particle assigned to a given lattice point is proportional to the area of a rectangle showed in the chart. For example, for a particle with coordinates x and y , a fraction $(l - x)(l - y)/l^2$ will be assigned to mesh point 1 and a fraction of xy/l^2 at mesh point 4 in Chart 1B (for simplicity, l is the length of the cell both in x and y directions). Thus, the density at every mesh point is the sum of all fractions assigned from all of the cells that share a given lattice point. According to the procedure described above, the size of the cell l is a parameter defining the density coarse-graining. The larger the value of l is, the higher the number of particles included in every cell and the coarser the calculated density will be. Once the coarse-grained density has been calculated from particle positions, the spatial derivatives of the density field can be evaluated. Spatial derivatives can be obtained by differentiation of the density lattice. In this way, the lattice where the derivatives are defined is staggered with respect to the lattice where the density is defined. As schematized in Chart 1B, the squares indicate the lattice points where the density is defined. Correspondingly, the density gradients are defined on the center of each edge (staggered lattice points indicated by crosses in Chart 1B) of the square surrounding the density lattice points.

Once both density and derivatives have been computed on their corresponding lattices, the potential energy and forces

Chart 1. (A) Construction of Coarse-Grained Density for a Phospholipid and (B) Criterion for the Assignment of Particle Fractions to Lattice Points

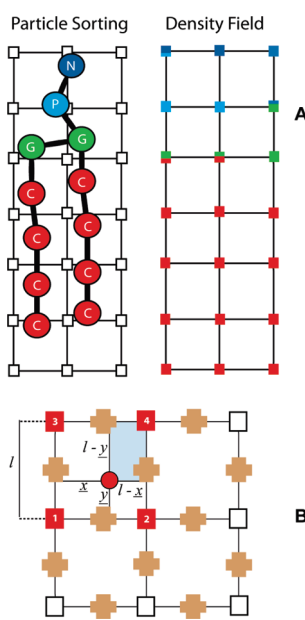


Table 1. Details about Simulated Systems

lipid type	box length ^a (nm)			composition			
	<i>x</i>	<i>y</i>	<i>z</i>	no. of lipids	no. of water	weight % lipids	T (K)
DPPC	8.17605	8.17605	6.94982	208	1600	60.9	325
DMPC	6.60390	6.60390	9.46884	208	1600	56.5	303
DOPC	7.21263	7.21263	9.62862	208	1600	64.5	303
DSPC	8.02782	8.02782	7.75874	208	1600	64.5	335

^aValues of box length in x , y , and z directions have been fixed using averages obtained from *NPT* simulations of the reference PP models.

acting on the particles can be calculated using values obtained by interpolation of the density and its spatial derivatives in eqs 8 and 9.

The iteration algorithm used in the MD-SCF approach is explained in the following. According to the initial configurations of the system (at time t_0), a starting value of the coarse-grained density is obtained. The coarse-grained density is defined on a lattice, and the values of the density and density gradients at the particles positions are calculated by linear interpolation. Then, from the density gradients, forces acting on the particles at position \mathbf{r} due to the interaction with the density fields are computed according to eq 9. The total force acting on the particles will be the sum of the intramolecular forces (bonds, angles, and intramolecular nonbonded forces calculated as in classical MD simulations) and the forces due to the interactions of particles with density fields. After the force calculation, a new configuration will be then obtained by integration of the equation of motion. In principle, for every new configuration, an update of the CG density calculated from the new coordinates should be performed. Test simulations have shown that, due to the collective nature of the density fields, it is possible to define an update frequency of the coarse-grained densities without a loss of accuracy.^{41,42} In other words, the values of the coarse-grained density at lattice points are not updated at every time step but only at every prefixed density update time (Δt_{update}). Then, between two updates, the values of the densities on the lattice used to interpolate both density and its derivatives will be constant. When an update of density is performed, a new coarse-grained density will be obtained, and the iteration algorithm converges when the coarse-grained density and the particle-field potential become self-consistent.

2.2. Simulations Details. Classical MD simulations used to obtain reference PP simulations have been performed using the program GROMACS (ver. 3.3).⁴³ The time step used for the integration of the equations of motion was 0.03 ps. The temperature and pressure were kept constant using Berendsen's weak coupling method ($\tau_T = 0.1$ ps and $\tau_P = 1$ ps). Target temperatures have been chosen according to the available experimental data and are listed in Table 1. A cutoff of 1.5 nm has been used to truncate nonbonded interactions. To equilibrate the system with *NPT* simulations, the target pressure was fixed to 1 bar, and semi-isotropic coupling has been employed. In order to achieve a better comparison between the results of PP and those of *NVT* PF simulations, *NVT* MD simulations have been performed using the average box lengths (see Table 1) obtained from the equilibrated *NPT* simulations. In particular, *NPT* simulations were performed for all systems for at least 120 ns. In the case of the DPPC lipid, the equilibrium area/lipid at 323 K for the PP model is 0.64 nm^2 . This value was reported by Marrink et al.⁴⁴ and is in agreement with the experimental value

reported by Nagle et al.⁴⁵ and later by Kučerka et al.⁴⁶ In order to simulate systems having a correct value of area/lipid, *NVT* PF simulations have been performed using average box lengths (see Table 1) that are corresponding to those obtained in the reference PP simulations.

The molecular dynamics program OCCAM⁴⁷ was used for hybrid particle-field MD simulations. PF simulations have been performed using a time step of 0.03 ps. *NVT* simulations have been conducted keeping the temperature constant using an Andersen thermostat with a collision frequency of 5 ps⁻¹.

All density profiles, for both PP and PF simulations, have been calculated from simulations equilibrated at least for 10 ns. Density profiles have been averaged over further 2 ns after equilibration. The composition of lipid water systems has been set in the range of stability of the bilayer phase. Details about systems sizes and compositions used in the simulations reported in this paper are summarized in Table 1.

3. MODELS AND THEIR PARAMETRIZATION

As described in section 2, according to the formulation of hybrid PF models, the intramolecular bonded interactions (bond, angles) can be modeled using usual force fields suitable for molecular simulations. Our choice is to develop a hybrid PF model based on a description able to retain the chemical specificity. The coarse-graining scheme proposed by Marrink and co-workers is suitable for this purpose. The advantages of this model are that the parametrization of the interaction potentials is not tailored to a specific lipid and different phospholipids can be modeled from a small set of bead types.

In Figure 1, the MARTINI coarse-graining mapping scheme of the atomistic structures is exemplified for the phospholipid dipalmitoylphosphatidylcholine (DPPC).

According to the formulation of the MD-SCF method, bond and angle interaction potentials have the same functional form and parameters as those in the original MARTINI force field.¹⁹ All types of nonbonded intramolecular interactions are assumed to be repulsive, while the intermolecular interactions are calculated using the assumption that each coarse-grained bead interacts with the density fields.

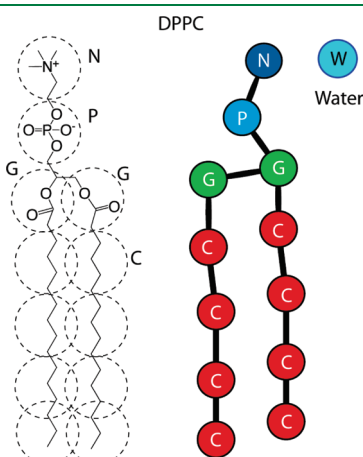


Figure 1. The adopted coarse-graining scheme for DPPC phospholipid is depicted. One coarse-grain bead corresponds to four atoms.

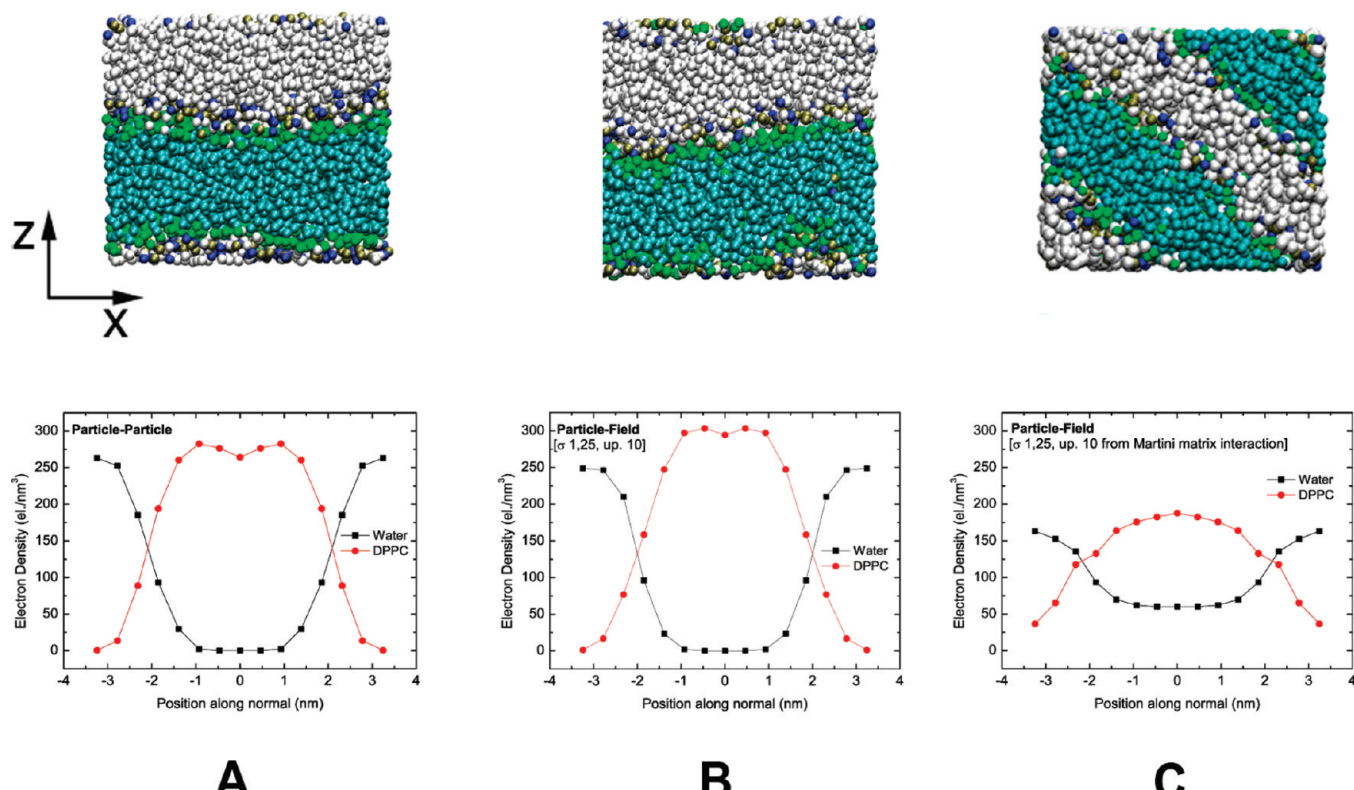


Figure 2. Water and DPPC density profiles and snapshot for (A) reference PP simulation, (B) PF simulation using a χ_{CW} parameter 2.5 times larger than the value calculated by eq 11, (C) PF simulation using the χ_{CW} parameter calculated by eq 11.

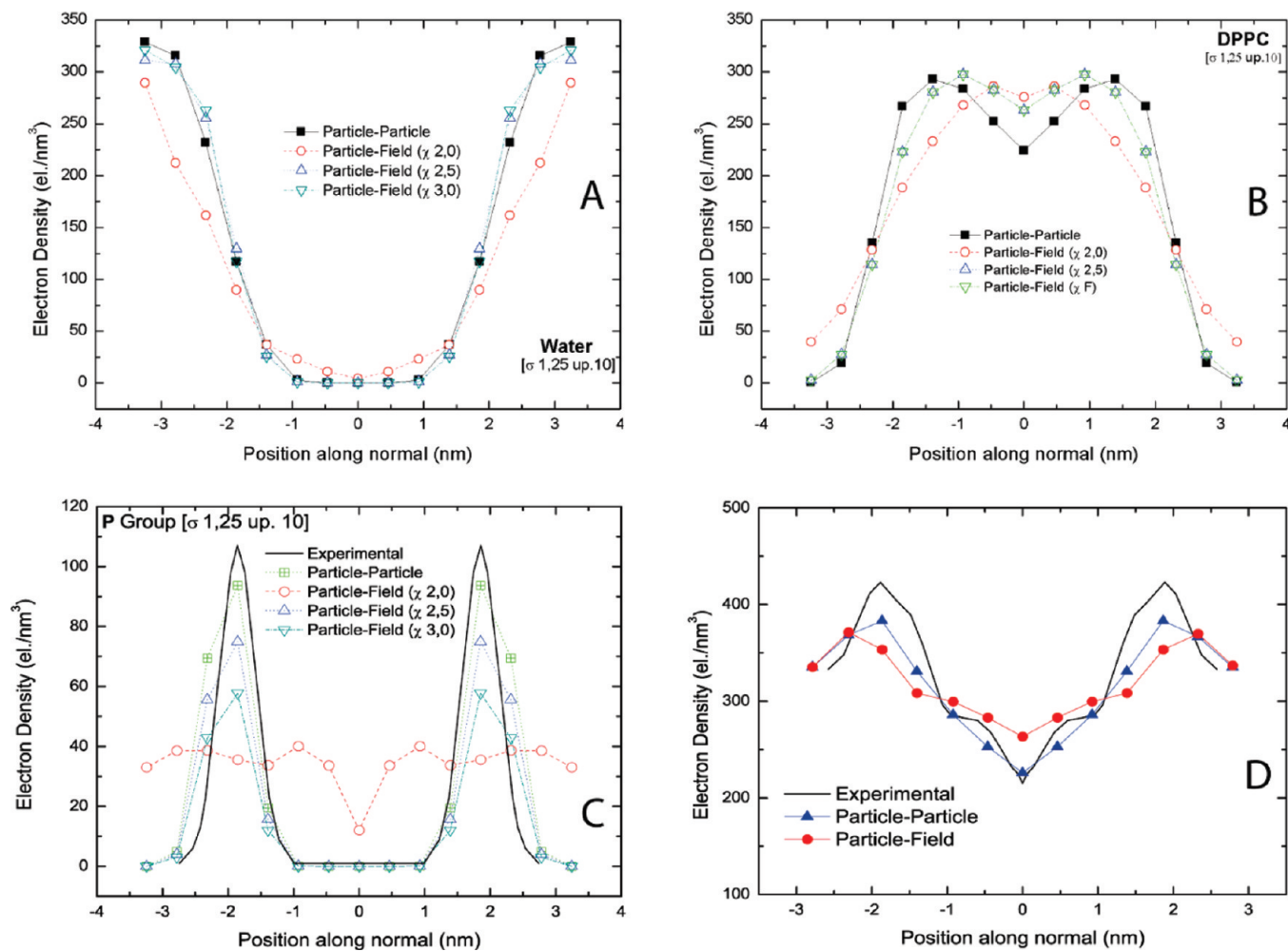


Figure 3. Comparison between reference PP and PF simulations using different values of the χ_{CW} parameter for electron density profiles of water (A), DPPC (B), and the phosphate group (C). Total density profiles for DPPC water system calculated from PP (red circles) and PF (blue triangles) simulations in comparison with experiments (black curves; D) are shown. The density profiles evaluated using the χ_{CW} parameter, which is scaled 2 to 3 times the value obtained from eq 11, are compared with those of the reference PP simulation.

According to eq 7, in order to calculate the PF potential, several mean field parameters $\chi_{KK'}$ between a particle of type K with the density field due to particles of type K' are needed. A simple choice of these parameters can be obtained by following the Flory–Huggins approach for the calculation of χ parameters for lattice models:

$$\chi_{KK'} = \frac{z_{\text{CN}}}{k_B T} \left[\frac{2u_{KK'} - (u_{KK} + u_{K'K'})}{2} \right] \quad (11)$$

where $u_{KK'}$ is the pairwise interaction energy between a pair of adjacent lattice sites occupied by the beads of types K and K' . These interaction energies have been set as $u_{KK'} = -\varepsilon_{KK'}$, where $\varepsilon_{KK'}$ is the Lennard-Jones ε parameter for the corresponding PP interactions. The parameter z_{CN} in eq 11 is the coordination number, which takes a value of 6 for a three-dimensional lattice. Another way to obtain the coordination number is from integration of the radial distribution function between all possible pairs. As the initial state for the MD simulations, we prepare a randomly mixed state of 208 DPPC and 1600 water molecules. Then, this mixture is subjected to an energy minimization procedure in order to avoid particle overlapping. This procedure gives an average number of neighbors per particle calculated at a

distance equal to 1.20σ close to 6.0. With the choices described above, it is possible, given the particle–particle ε parameters and the value of z_{CN} , to obtain the corresponding PF parameters. According to our choice, the χ parameters have been obtained considering the interactions between the different particle types classified according to the four types polar, nonpolar, apolar, and charged interactions considered in the MARTINI force field.¹⁹

Using the models and the PF parameters described above, we simulated a system of DPPC and water using small values of both grid size ($l = 0.587$ nm, corresponding to 1.25σ) and update frequency (0.3 ps, corresponding to 10 time steps).

In order to determine the value of the parameter κ , which regulates the strength of the incompressibility condition imposed in eq 10, we analyzed the behavior of density fluctuations in the reference PP simulation. The criterion is the reproduction of the value of the average density fluctuations, calculated as mean square deviation between the average total density and instantaneous value averaged over all lattice points using the same grid size used in PF simulations. In particular, using values of $1/\kappa$ of about $8RT$ (where R is the gas constant and T temperature), average density fluctuations, in agreement with the reference PP simulation, are found to be smaller than 1%.

Table 2. Particle-Field Interaction Matrix^a

	N	P	G	C	D	W
N	0.00	-1.50	6.30	9.00	7.20	-8.10
P	-1.50	0.00	4.50	13.50	11.70	-3.60
G	6.30	4.50	0.00	6.30	6.30	4.50
C	9.00	13.50	6.30	0.00	0.00	33.75
D	7.20	11.70	6.30	0.00	0.00	23.25
W	-8.10	-3.60	4.50	33.75	23.25	0.00

^a $\chi_{KK'} \times RT$ (kJ/mol) for particles of type K interacting with density field due to particle of type K' are reported. χ parameters have been calculated using eq 11; the value of χ_{CW} is 2.5 times the one calculated by eq 11.

The system has been simulated for 60 ns; further details about simulations have been reported in section 2. In Figure 2, snapshots of the simulations together with calculated electron density profiles are reported. Here, the electron density profiles are obtained by multiplying the particle number density by the number of electrons contained in a given bead. As shown in Figure 2C, similarly to the reference PP simulation, the hybrid PF simulation leads to a successful formation of a lipid bilayer. Further comparisons between the results of PP and PF MD simulation have been used to refine the set of initial χ parameters obtained using eq 11.

In Figure 2, electron density profiles calculated by PP and PF MD simulations for the DPPC/water system (bottom panel of Figure 2) have been compared.

From a comparison of the density profiles of Figures 2A and B, it is clear that the PF model gives a weaker phase separation between DPPC and water molecules with respect to the MD simulation. Furthermore, the snapshot of Figure 2C shows that, for the system simulated with the hybrid PF method, the phospholipid plane lies along the diagonal of the simulation box. This indicates the tendency of the lipid molecules to occupy a larger area for the lipid. This tendency can be connected to a different size of the lipid molecules in the PF simulations from that of the PP simulations. To show this, the radius of gyration and the angle between two tails obtained from PP and PF simulations have been compared. In particular, histograms of these two structural quantities are very similar for both models (see the Supporting Information). As a result, both weak phase separation between the lipid and water and the tendency to occupy a larger area per lipid can be mainly ascribed to an underestimation of repulsion between the DPPC molecules and water in PF models with respect to PP ones. Following this idea, several simulations were conducted to refine the interaction parameter between the hydrophobic tails of lipids and water molecules (namely the χ_{CW} parameter). Test simulations show that starting from values of χ_{CW} parameter 2.5 times larger than the value calculated by eq 11, the lipid bilayer does not occupy a larger area per lipid than the PP simulations and lies parallel to the xy plane of the simulation box. In Figure 3, density profiles of DPPC, water, and the phosphate group (P) obtained from simulations in which the repulsion between water and hydrophobic tail is further increased to 3 times that obtained with eq 11 are reported.

From Figure 3, it is clear that using a value of the χ_{CW} parameter that is 2.5 times larger than that evaluated by eq 11 gives electron density profiles very close to that in the reference PP simulations. In Figure 3D, the total electron density profiles of the DPPC/water system calculated from PP and PF simulations are compared with those obtained by fitting X-ray diffraction

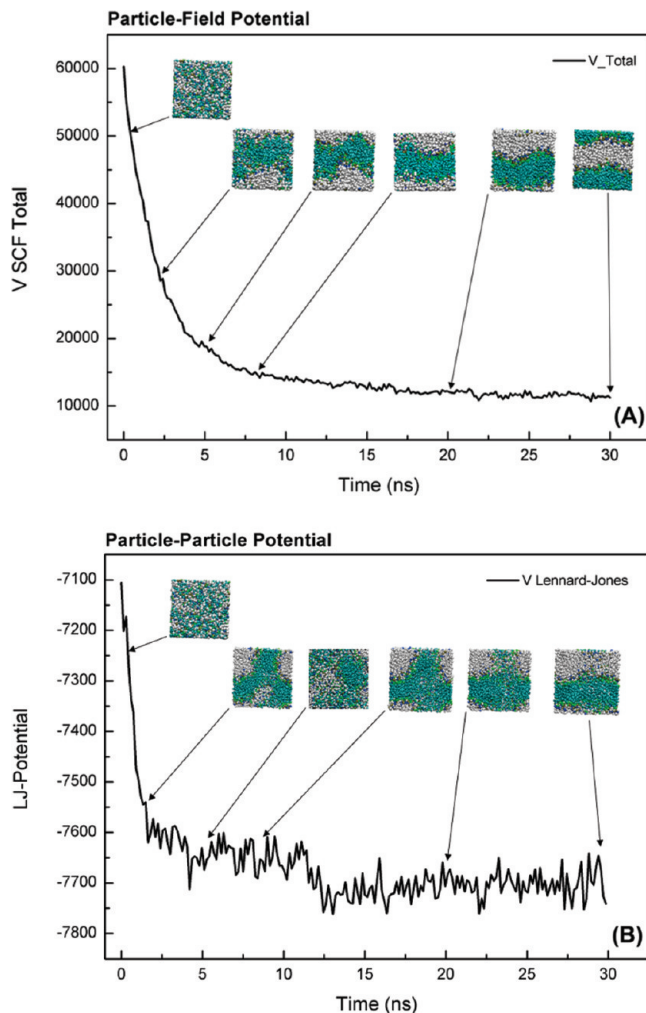


Figure 4. Comparison of the self-assembly process of DPPC and water in a bilayer phase obtained from PF (A) and PP simulations (B). In the figure, the time behavior of particle-field intermolecular potential in the PF MD simulation is compared with the behavior of the nonbonded Lennard-Jones potential in the PP MD simulation. Potential units are kilojoules per mole.

experiments of Kučerka and co-workers.⁴⁶ The behavior of the calculated density profiles is smoother than the experimental one. In particular, in both PP and PF density profiles, the height of the peaks located at about 2 nm from the center of the bilayer is slightly underestimated. This effect, similar in PP and PF simulations, can be ascribed more to the coarse-grained nature of the models (reduction of degrees of freedom into one effective bead) than to the field description in the hybrid PF models; a similar behavior is found comparing the behavior of the calculated and experimental density profiles for the phosphate group (Figure 3C). The optimized set of χ parameters for all PF interactions is reported in Table 2.

According to eq 11, the interaction matrix is symmetric, and the χ parameter between the same type of particles is zero.

4. SIMULATIONS RESULTS

In Figure 4, self-assemblies of DPPC/water systems simulated using PP and PF models are compared. For both simulations, the initial configuration and the simulation conditions are the same

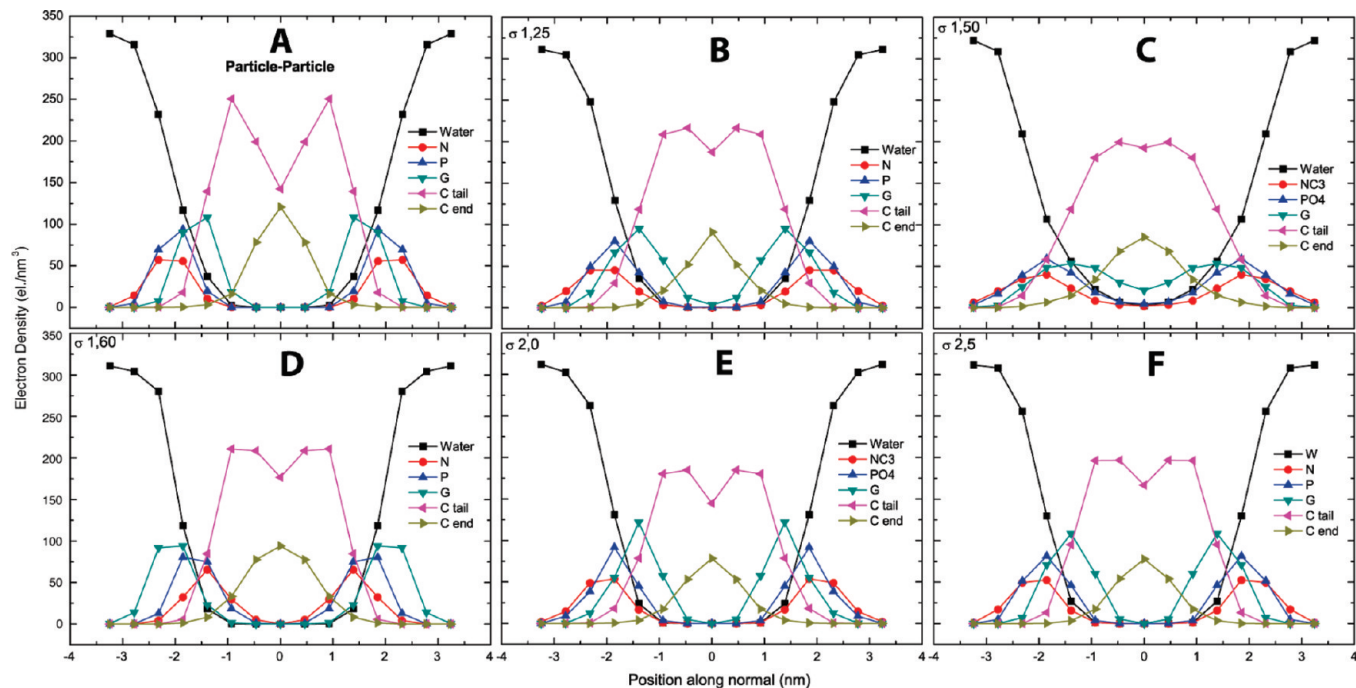


Figure 5. Partial density profiles for water and DPPC obtained from (A) PP simulations and PF simulations using $l =$ (B) 1.25σ , (C) 1.50σ , (D) 1.60σ , (E) 2.0σ , and (F) 2.5σ . In all PF simulations, the update frequency Δt_{update} is 10 time steps.

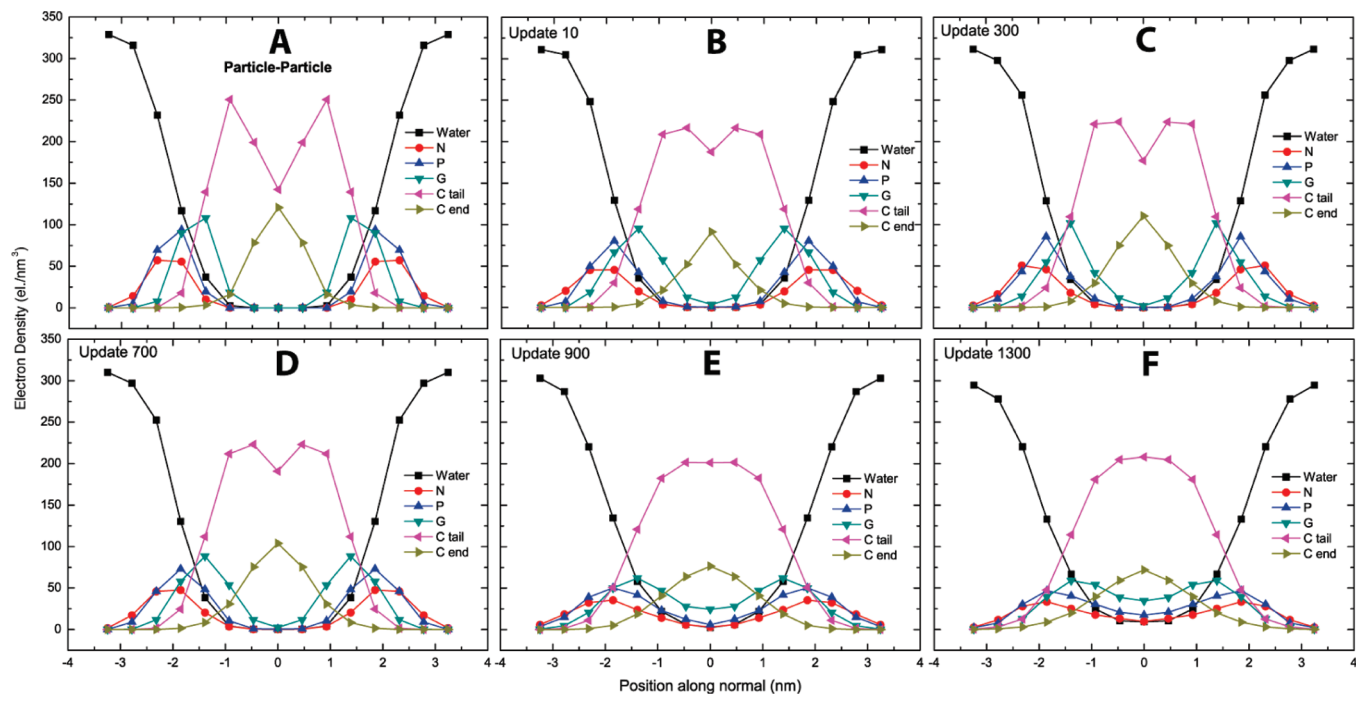


Figure 6. Partial density profiles for water and DPPC obtained from (A) PP simulations and PF simulations using $\Delta t_{\text{update}} =$ (B) 10, (C) 300, (D) 700, (E) 900, and (F) 1300 time steps. In all PF simulations, the grid size l is 1.25σ .

(see Table 1). The starting configuration for both simulations is made up of randomly mixed DPPC and water molecules.

It is worth noting that in the PF simulations the formation of the lipid bilayer as stable equilibrium state, as shown by the snapshots reported in Figure 4A, is observed already after about 7 ns. From Figure 4B it can be noted that in the same time interval

the PP simulation shows only an initial stage of phase separation and a stable lipid bilayer phase is formed only after 30 ns.

4.1. Influence of Density Coarse-Graining. *4.1.1. Structural Properties.* As described in section 2, coarse-grained density fields $\phi_K(\mathbf{r})$, obtained from particle positions for every particle type K , are used to calculate PF potentials and forces using eqs 8 and 9.

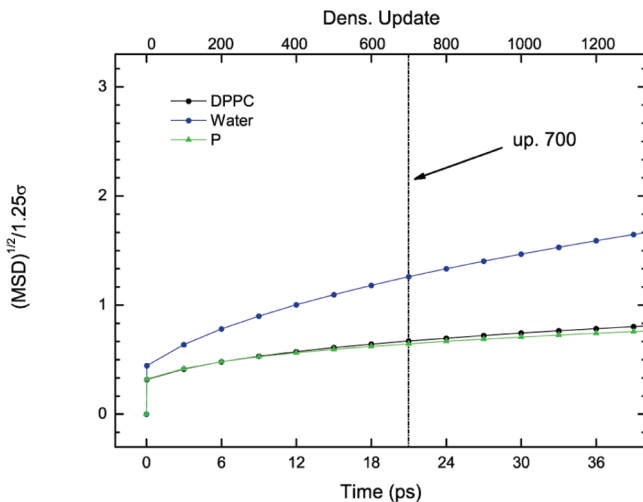


Figure 7. Normalized displacement of water, DPPC, and P beads as a function of time.

According to the scheme described above, two parameters, the cell size l and the update frequency Δt_{update} , regulate the degree of coarse-graining of the density fields. Larger cell sizes lead to more collective density fields. As for the value of the update frequency, it has to be chosen in a way that the approximation of slow variation of the field with respect to the particle displacement is valid between two density updates. In this section, simulation results using different density update frequencies and cell sizes will be discussed and compared with the results of reference PP simulations.

Several test simulations have been performed to understand the effect of the cell size l on the quality of calculated electron density profiles of the DPPC water bilayer. In Figure 5, partial density profiles corresponding to water and to the four different bead types (N, P, G, and C) present in DPPC obtained using l ranging from 1.25 and 2.5σ (corresponding to 0.59 and 1.17 nm) and using the same update frequency ($\Delta t_{\text{update}} = 10$ timesteps) are reported. From Figure 5 it is clear that PF simulations reproduce the structure of the lipid bilayer phase obtained from reference PP simulations well (Figure 5A). Values of l larger than 2.5σ give rise to stronger phase separation between water and DPPC with a narrowing of the density profiles. The grid size is larger, and this effect is more pronounced.

In Figure 6, electron partial density profiles for a mixture of water and DPPC molecules obtained for different values of the density update and using the same grid size ($l = 1.25 \sigma$) are compared with those obtained from reference PP simulations. In particular, the behaviors for Δt_{update} ranging from 10 (0.3 ps) to 1300 (39 ps) time steps are compared.

As expected, the agreement between PP and PF density profiles worsens as the Δt_{update} grows. For an update frequency between 10 and 700 time steps, water and DPPC density profiles are quite similar (see Figure 6B–D) and reproduce the behavior of the reference PP simulation well. Starting from update frequencies of 900 time steps (see Figure 6E), artificial undulations in the lipid bilayers are obtained. This causes a smoothing of the calculated density profiles. In particular, when large updates are used, the central depletion in the density profile of the hydrophobic beads of type C is absent (Figures 6E,F). Furthermore, the density profiles of the DPPC head groups N and P and of the bead types G are very shallow (Figure 6E,F).

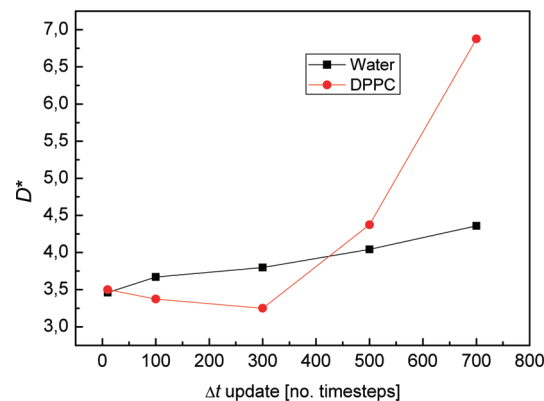


Figure 8. Ratio between PP and PF diffusion coefficients as a function of the update frequency calculated for water (black curve) and DPPC (red curve).

The reproduction of the spatial organization of the head groups and in particular the phosphate group (type P) is important for the quality of the model. In fact, the bilayer thickness (D_{HH}), obtained by calculating the distance between the two peaks of the density profile corresponding to the phosphate group, can be compared with the values obtained from X-ray and/or neutron diffraction measurements. In the case of DPPC at 323 K (50 °C), a value of D_{HH} of 3.7 nm is obtained from PF simulations using update frequencies from 10 to 700 time steps. This value is equal to the one obtained from PP simulations and close to the experimental value of 3.8 nm measured at the same temperature.⁴⁸ For larger values of density update frequency, the electron density profile of P groups becomes broader, and a correct evaluation of D_{HH} becomes unreliable.

In order to understand the behavior of the systems as a function of the frequency of the density update, it is useful to compare the mean square displacement (MSD) of the particles as a function of time. In Figure 7, we present the behavior of the square root of the mean square displacement for water and the DPPC in units of cell length ($((MSD)^{1/2})/l$ where l is the cell length) as function of time for different values of update frequencies.

This is a direct way to understand the validity of the approximation of slow variation of the field with respect to the particle displacement between two density updates. In fact, the plot of Figure 7 quantifies how many cells a particle can cross in a given amount of simulation time. From Figure 7, it is clear that for update frequencies between 500 and 700 steps (corresponding to 15 and 21 ps) both water and DPPC beads have a displacement smaller than or equal to the cell size. For larger update time intervals, the displacement is larger than the size of a cell. This result agrees well with the good reproduction of density profiles and a bilayer thickness for update frequencies smaller than 700 steps.

This kind of analysis of PF simulations can be useful in general to set a suitable value for the update frequency also in the absence of reference simulations data.

4.1.2. Dynamical Properties. From the comparison of the self-assembly processes of a lipid bilayer obtained in the simulations shown in Figure 4, it is clear that the dynamics of the system simulated by the PF method are faster. This is due to smoother potentials and forces characterizing the PF Hamiltonian. In particular, PF models include the effect of excluded volume

Table 3. Diffusion Coefficients Calculated Using Different Update Frequencies^a

update frequency [timesteps]	water [$\text{cm}^2/\text{s} \times 10^5$]				DPPC [$\text{cm}^2/\text{s} \times 10^5$]			
	total	<i>x</i>	<i>y</i>	<i>z</i>	total	<i>x</i>	<i>y</i>	<i>z</i>
particle-particle	1.27	1.63	1.63	0.43	0.08	0.13	0.12	0.01
10	4.40	6.5	6.6	0.04	0.28	0.45	0.43	0.03
100	4.67	7.1	6.8	0.04	0.27	0.43	0.44	0.03
300	4.82	7.3	7.1	0.04	0.26	0.38	0.38	0.04
500	5.13	7.6	7.6	0.05	0.35	0.52	0.50	0.03
700	5.53	8.4	8.4	0.05	0.55	0.079	0.078	0.09

^a The grid size l is equal to 1.25σ for all simulations.

interactions between particles using the incompressibility condition described in eq 7. Forces acting on the particles then depend on the derivatives of the density fields that change smoothly over the length scale at larger than average distances between particle pairs.

In order to compare more quantitatively the different dynamics in PP and PF simulations, diffusion coefficients have been calculated from the MSD behaviors of water and DPPC particles as functions of time.

In Figure 8, values of the ratio D^* between the diffusion coefficients calculated from the PF simulations using different update frequencies and the one calculated from the reference PP simulation are reported. In all of the cases and for both water and DPPC, the diffusion coefficients calculated from the results of PF simulations are larger than those obtained from the results of the PP simulation. The diffusion of water is 3.5 to 4 times faster for PF simulations. The increase of the diffusion coefficient of the DPPC lipid ranges from about 3.5 to 7 times the value obtained from the reference PP simulation. This behavior is in agreement with the faster formation of a stable lipid bilayer as obtained from the comparison between PF and PP simulations reported in Figure 4.

In Table 3, the values of diffusion coefficients and their components calculated from PP and PF simulations using different density update frequencies are reported.

Results of the test simulations obtained using different grid sizes l and the same update frequency (300 timesteps) are reported in Figure 9. In particular, the values of the diffusion coefficients of water and DPPC increase according to the increase in the grid size. This is reasonable because a coarser density will give rise to smoother particle-field potentials and forces.

In the case of water, there is a small decrease in the diffusion coefficient for the largest grid sizes (2.0σ). This effect is due to the deviation from the reference density profile obtained when a larger grid size is used. As described in the previous paragraph, large grid sizes give rise to stronger phase separation between water and DPPC. The *x* and *y* components of the diffusion tensor of the water parallel to the bilayer plane show small variation as a function of the grid size, and they are practically constant within the error bar. In contrast, the *z* component of the diffusion tensor of water going from a grid size of 1.5 to 2.0σ is reduced by a factor of 2.

4.2. Particle–Particle and Particle–Field Correlations. The formulation of the hybrid MD-SCF method employed here is based on the interactions of single molecules with external density fields. Interactions between different molecules do not involve the evaluation of forces between particle pairs. This implies that, although the density profiles calculated with PF and

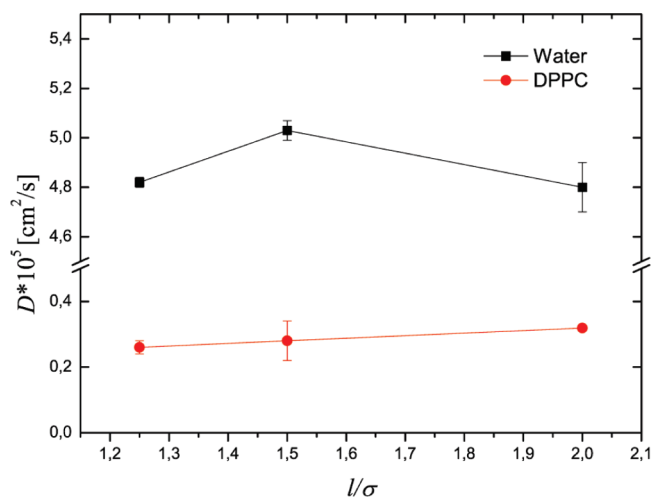


Figure 9. Behavior diffusion coefficients of water and DPPC as a function of the CG density grid size.

PP simulations are in good agreement, pair correlations between particles can be different.

In the case of PP simulations, the equilibrium structure and then the density profiles are the result of excluded volume interactions and of the different pair forces between hydrophilic and hydrophobic beads. In the case of PF simulations, the structure and the density profiles obtained from simulations are the result of the different interactions between every single hydrophilic and hydrophobic particle and the density external fields. To illustrate this point intuitively, we compare the radial distribution functions for several bead types between PP and PF simulations. Red curves in Figures 10 and 11 correspond to the radial distribution functions calculated in simulations where the short-range particle–particle repulsive interactions are explicitly included in the PF model. These simulations, named particle–particle particle–field (PPPF), will be discussed later.

In Figure 10A, radial distribution functions ($g(r)$) between the beads of water and hydrophobic tail beads (type C) calculated from PP (black curve) and PF (blue curve) simulations are shown.

For these particle pairs, the main features of $g(r)$ for the PP and PF simulations are very similar, except that the behavior of the PF is a bit smoother than that of the PP simulations.

This is due to smoother interactions between water particles and the field generated by the hydrophobic tail particles. Still similar is the behavior of the $g(r)$ between water and G type beads (Figure 10B). In this case, the radial distribution functions of the PF simulations, due to the continuous nature of the field

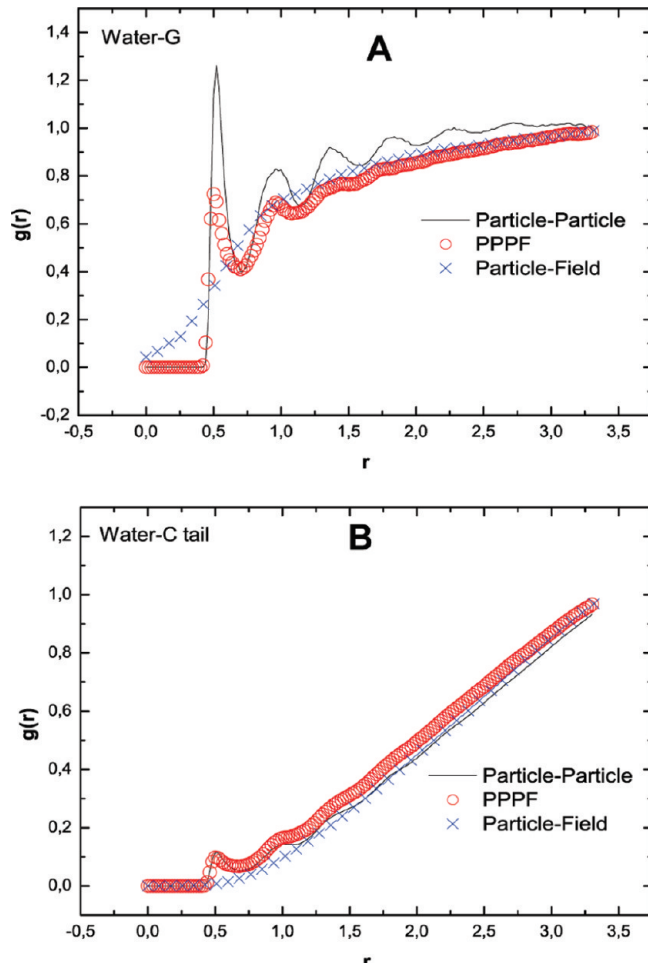


Figure 10. Radial distribution functions for (A) water–G tail and (B) water–C tail pairs.

representation, are characterized by the absence of peaks and a smoother behavior. Furthermore, at zero distance, the PF $g(r)$ shows a small nonzero value. Differently from PP simulations, where the overlapping between particles is strictly avoided, in the PF simulations, the excluded volume effects between different particles are taken into account in the field description by imposing the incompressibility condition in eq 7.

Different is the behavior of particle correlations in lipid and water pure phases. In particular, in Figure 11A, $g(r)$ between DPPC beads and, in Figure 11B, $g(r)$ between the water beads, both of which are obtained in PP and PF simulations, are compared.

In this case, at the PF level, the absence of correlations between particles is clear from the behavior of $g(r)$ between both water and DPPC pairs. The absence of direct correlation between particle pairs, as has been found in the radial distribution functions of Figure 11, is what is expected according to the formulation of the PF method. Differently from PP simulations, the Hamiltonian employed in PF simulations does not involve terms depending on the distance between particle pairs. The only correlation expected is between the particle and fields. In fact, this correlation has been found in the case of water and the field due to the C hydrophobic beads and partially in the case of water and the field due to G-type particles. Also in this case, due to the formulation of the PF method, although a direct correlation between the pair is still absent, the behavior of radial distribution

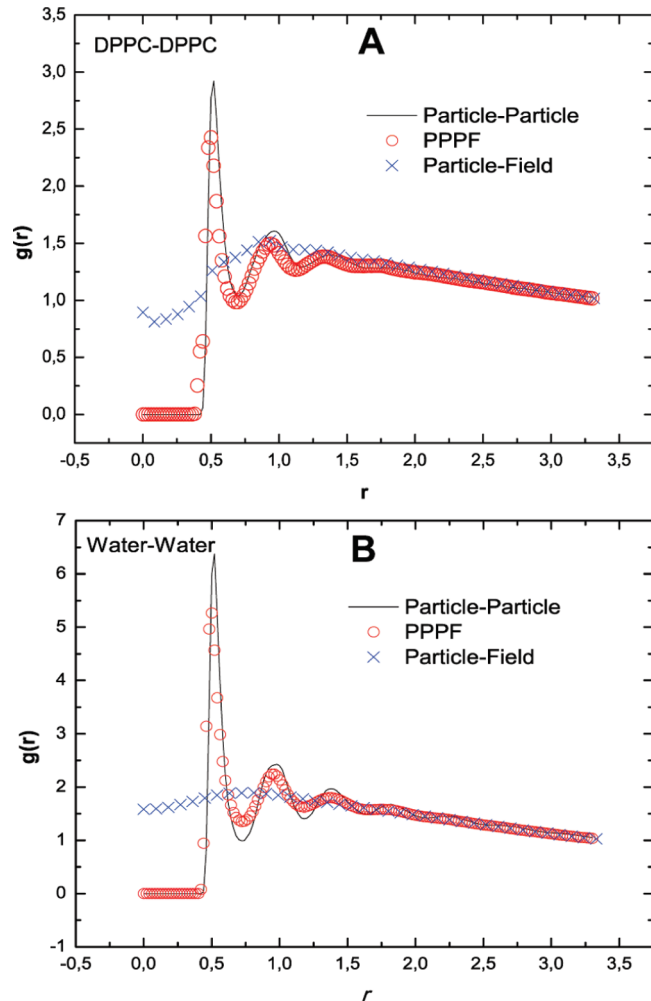


Figure 11. Radial distribution functions obtained from PP (black curve), PF (blue curve), and PPPF (red curve) simulations for (A) DPPC–DPPC and (B) water–water pairs.

functions is only a consequence of the repulsive interactions between water particles and density fields obtained from C or G particle types that lead to a phase separated system.

On the contrary, as shown in Figure 11, a direct correlation between particles belonging to the same hydrophilic or hydrophobic phase is absent. In the case of PP simulations, short-range correlations are dominated by excluded volume interactions due to the repulsive part of Lennard-Jones potentials between particle pairs. In contrast, in PF simulations, excluded volume interactions are modeled at the density field level by applying the incompressibility condition included in the second addend of eq 7. In this case, the density is kept homogeneous in all systems, and it is allowed to fluctuate according to the value of compressibility κ (eq 7).

In Figures 10 and 11, the behaviors of the $g(r)$ obtained from PPPF simulations are also reported as red points.

In the simulations named PPPF, particle–field interaction potential has the form of eq 7 but without inclusion of the incompressibility condition. The excluded volume intermolecular interactions are then modeled by truncated short-range Lennard-Jones potentials. In this case, intermolecular short-range interactions are included at the particle–particle level as purely repulsive Lennard-Jones potentials truncated at $\sigma_{\min} = 2^{1/6}\sigma$,

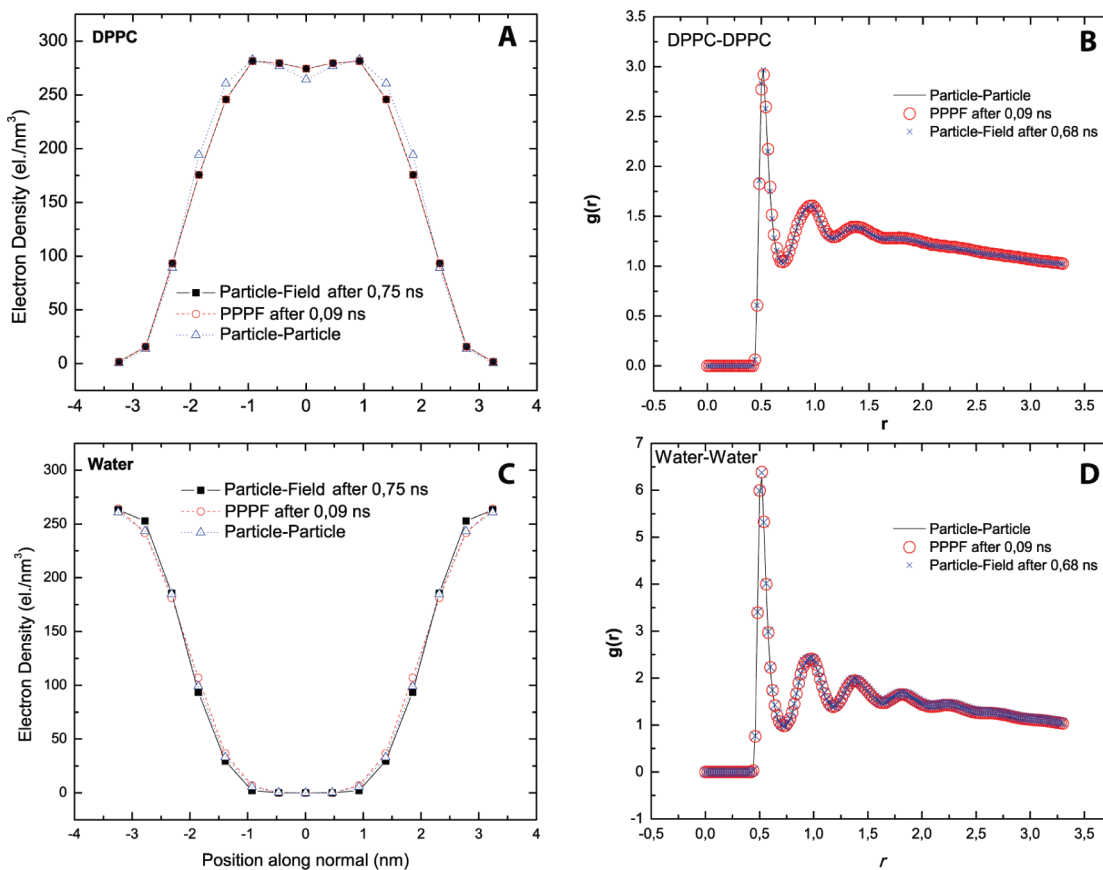


Figure 12. Comparison between PP and reverse mapped (A) DPPC and (C) water density profiles. DPPC–DPPC (B) and water–water (D) radial distribution functions. Results obtained from full equilibration at the PP level (black curves) are compared with ones obtained from reverse-mapped configurations at the PF (blue cross) and PPPF (red circles) levels.

while long-range interactions are still modeled with interactions between the particle and fields. The PPPF simulations have been run starting from equilibrium configurations obtained from PF simulations. The excluded volume pair interactions have been first gradually introduced by scaling both ϵ and σ from 0.001 to their full values in a few hundred steps and then running simulations with full values of ϵ and σ and with electrostatic interactions for about 2000 steps. From Figure 11, it is clear that short-range correlations between particles of PP simulations can be fully recovered at the PPPF level with very similar radial distribution functions.

4.3. Reverse Mapping: From PF to PP Configurations. One of the important uses of CG models is to obtain well-relaxed structures useful for generating configurations at a higher level of chemical detail. An example is the generation by local relaxation of structures of dense polymer melts at the atomistic level starting from mesoscale models.^{49–51}

In the present case, the coarse-graining process operated from PP to PF models does not involve the reduction of the number of simulated particles, and shown above, the information that is averaged out is the direct correlation between particle pairs.

The procedure of PP simulations → derivation of a PF model; PF simulations → reverse-mapping and local relaxation of PP models can be an efficient way to obtain well-relaxed configurations of large systems suitable for full MD simulations. From this point of view, it is interesting to understand how easy it can be for the systems under investigation to reach an equilibrium structure that is indistinguishable from the one obtained by long PP

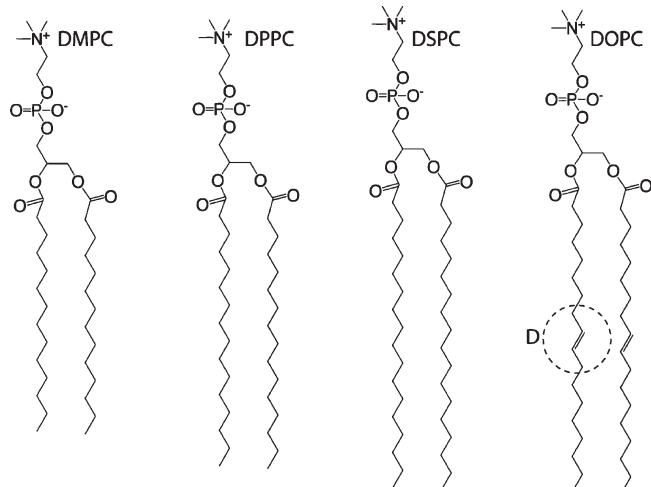


Figure 13. Structure formulas of the four phospholipids considered in the present study. The mapping scheme adopted for the CG models is the one depicted in Figure 1. For the DOPC phospholipid, the mapping for beads of type D including carbon atoms involved in double bonds is shown.

simulations starting from PF or PPPF configurations. This information is useful for evaluating the feasibility of a possible reverse mapping procedure able to give systems configurations suitable for the production runs of PP simulations.

Tests using classical PP MD simulations aimed to relax configurations equilibrated at the PF (only in this case, the configurations have been previously optimized for about 300 steps) and at PPPF (no optimization has been employed in this case) levels have been conducted. These test runs show that, starting from configurations relaxed at the PF level, about 20 000 steps (corresponding to about 0.7 ns) are needed to obtain well relaxed structures equivalent to the fully equilibrated state of the PP simulations. In the case of configurations coming from PPPF, shorter simulations of about 3000 steps (corresponding to 90 ps) are required. In Figure 12, the radial distribution functions and density profiles obtained from reverse mapping procedures and the ones obtained by full equilibration at the PP level are compared. From the figure, it is clear that the structures obtained are indistinguishable, and both $g(r)$ and density profiles are practically identical.

4.4. Extension to other Phospholipids. One of the advantages of our reference PP coarse-grained model is that the parametrization of the interaction potentials is not tailored to a specific lipid, and different phospholipids can be modeled, taking

Table 4. Deviations S_k (el/nm³) between Particle–Particle and Particle–Field Density Profiles for All Considered Lipids

lipid	S_W^a	S_P^a	S_C^a	average %
DPPC	8.5 (9.4%) ^b	4.3 (17%) ^b	16.5 (19.8%) ^b	15%
DMPC	18.3 (11%) ^b	7.4 (33%) ^b	12.6 (17%) ^b	20%
DSPC	7.2 (5.6%) ^b	10.9 (46%) ^b	11.4 (11%) ^b	21%
DOPC	16.9 (13%) ^b	8.9 (38%) ^b	17.3 (16%) ^b	22%

^a Deviations have been calculated using particle–field density profiles obtained using grid size $l = 1.25\sigma$ and an update frequency of 10 time steps. ^b Deviation calculated as a percentage $S_k/\rho_{k\text{aver}} \times 100$ of the average density of the species, where $\rho_{k\text{aver}}$ is the average electron density of the species k .

into account different chemical structures, using a small set of bead types.

In this section, simulations aiming to test the transferability of the model developed for DPPC and the relative PF $\chi_{KK'}$ parameters are reported. Electron density profiles and bilayer thickness are compared between PF and PP models and with experiments.

In particular, further test simulations are conducted for three biologically relevant lipids, i.e. dimyristoylphosphatidylcholine (DMPC), distearoylphosphatidylcholine (DSPC), and dioleoylphosphatidylcholine (DOPC). In Figure 13, the chemical structures of these three phospholipids are shown along with the structure of DPPC.

The advantage of our reference PP coarse-grained models lies in the straightforward way in which the corresponding atomistic structure can be represented. The differences between lipids depend on the molecular structure on the atomistic level. For instance, the main difference between DMPC, DPPC, and DSPC is in the numbers of carbon atoms present in the hydrophobic tails. In this case, at the CG level, the PP models differ only in the number of beads of type C (see Figures 1 and 13) that compose the tails, while the parameters for the nonbonded bond and angle potentials are the same. Differently, in the case of DOPC, the presence of a double bond in each hydrophobic chain requires an extra particle type corresponding to four atoms including a double bond (see Figure 13, particle type D). For this reason, in the DOPC CG model, some of the angles and nonbonded potentials are different. In particular, the C–C–C harmonic angle potential has a minimum at 180°, while the C–D–C harmonic angle potential has a minimum at 120°. In the same way, nonbonded interactions of beads of types C and D are different.

Correspondingly, the particle–field models of DMPC, DPPC, and DSPC have the same bonded, intramolecular nonbonded, and the χ (see Table 2) parameters, and they differ only in the

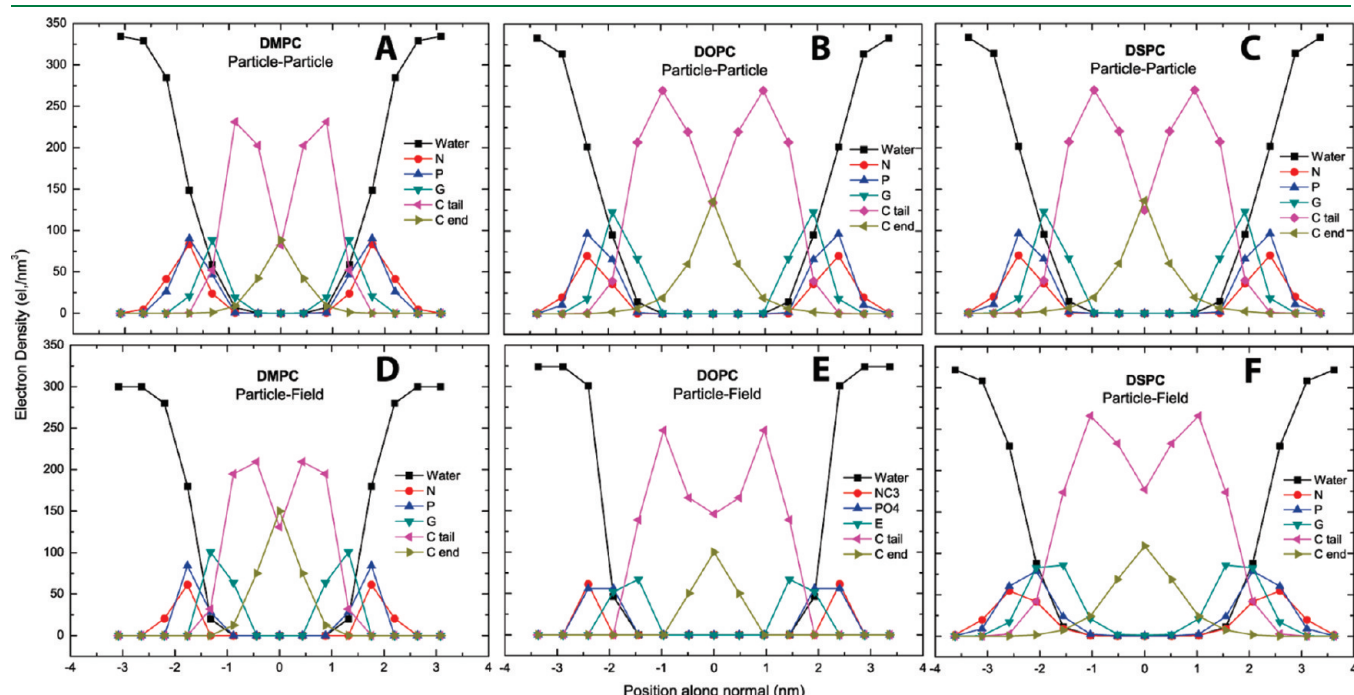


Figure 14. Electron density profiles calculated for DMPC, DOPC, and DSPC lipids with PF and PP simulations. Simulations for each lipid have been performed at the temperatures listed in Table 5.

number of beads. In the case of DOPC, having an extra bead type D and particle–field interactions involving only this new bead type introduces the use of different χ parameters. Of course, the interactions involving beads of type C are treated in the same manner as in DMPC, DPPC, and DSPC lipids. A complete list of parameters for the intramolecular interactions is reported in the Supporting Information.

Other details about simulated systems are reported in Table 1. Simulation temperatures have been chosen according to the available experimental data; temperatures of both experiments and simulations are listed in Table 4.

From these simulations, partial electron density profiles and bilayer thicknesses (D_{HH}) have been calculated and compared with those of the reference PP simulations and available experimental data.^{45,48,52}

Partial electron density profiles compared with the corresponding ones obtained from particle–particle simulations are shown in Figure 14.

Table 5. Deviations S_k (el/nm³) between DMPC and DOPC Density Profiles

model	S_W	S_P	S_C	average %
particle–particle	29.0 (22%) ^a	21.6 (99%) ^a	39.5 (44%) ^a	55%
particle–field ^b	30.0 (24%) ^a	16.0 (73%) ^a	30.0 (34%) ^a	49%

^a Deviation calculated as a percentage $S_k/\rho_k^{\text{aver}} \times 100$ of the average density of the species, where ρ_k^{aver} is the average electron density of the species k . ^b Deviations for particle–field density profiles have been calculated using using grid size $l = 1.25\sigma$ and an update frequency of 10 time steps.

Table 6. Calculated Bilayer Thickness^a

phospholipid	D_{HH} particle–particle (nm)	D_{HH} particle–field (nm)	D_{HH} experimental (nm)
DMPC	3.7 (30 °C)	3.7 (30 °C)	3.8 ^b –3.5 ^c (30 °C)
DPPC	3.5 (50 °C)	3.5 (50 °C)	3.6 ^b (50 °C)
DOPC	4.1 (30 °C)	4.0 (30 °C)	3.7 ^b –3.6 ^d (30 °C)
DSPC	4.1 (60 °C)	4.4 (60 °C)	4.0 ^b –4.1 ^c (60 °C)

^a Simulations have been performed at temperatures corresponding to the available experimental data. ^b From ref 48. ^c From ref 52. ^d From ref 53. ^e From ref 54.

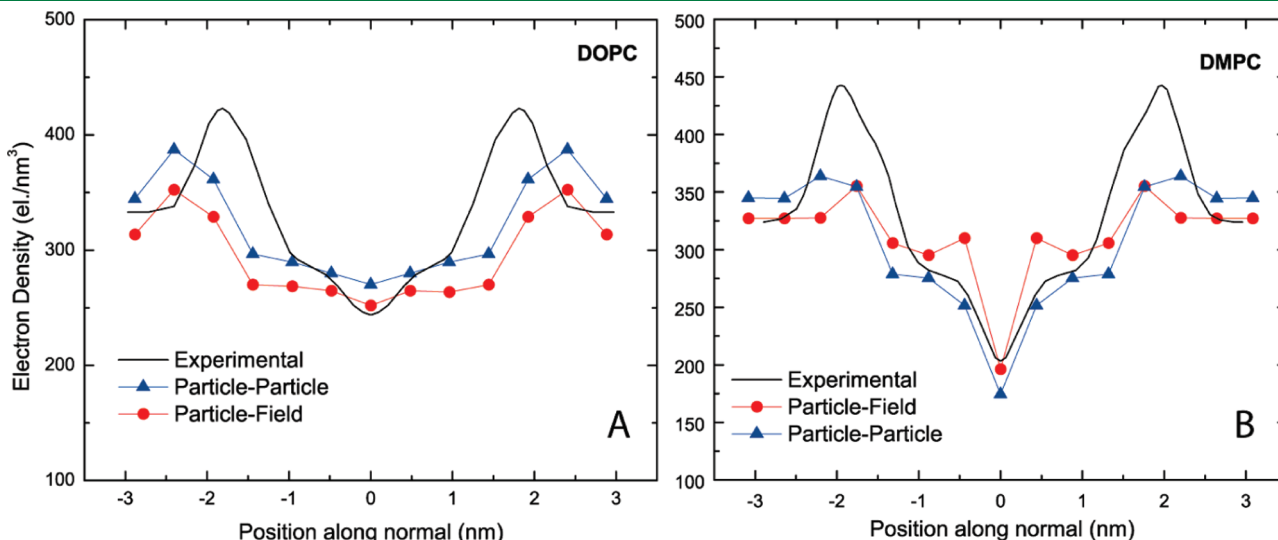


Figure 15. Total electron density profiles for DOPC (A) and DMPC (B) lipids.

From Figure 14, it is possible to see that in all cases there is a good agreement between the density profiles of the reference PP and PF models. In order to evaluate quantitatively the difference between the reference density profile and the one calculated from particle–field simulations for a given bead type k , the following evaluation function can be defined:

$$S_k = \frac{1}{2l_z} \int_{-l_z}^{+l_z} |\Delta\rho_k(z)| dz \quad (12)$$

where $\Delta\rho_k(z)$ is the difference between the values of the density calculated with the particle field and the reference particle–particle models for a given particle type k . According to the definition given above, in Table 4, the values of S_W , S_P , and S_C (in el/nm³ as units) obtained by comparing PP and PF density profiles for all considered lipids are reported. The average deviation is smaller for DPPC (15%), and this is not surprising because the PP density profile of this lipid has been used for the parametrization of PF interactions. Interestingly, also the deviations between PP and PF density profiles for the other lipids are similar (around 20%). Furthermore, the main differences between the density profiles of different lipids calculated in the PP simulations can be reproduced by the PF model. For example, a comparison between DMPC and DOPC density profiles can be done using the deviations S_k . In Table 5, the deviation between density profiles of DMPC and DOPC are reported for both PP and PF simulations. It is worth noting than in this case the deviations (on the order of 50%) are much larger than the ones calculated between PP and PF density profiles of the same lipids. Furthermore, the values obtained for the deviations for single species is

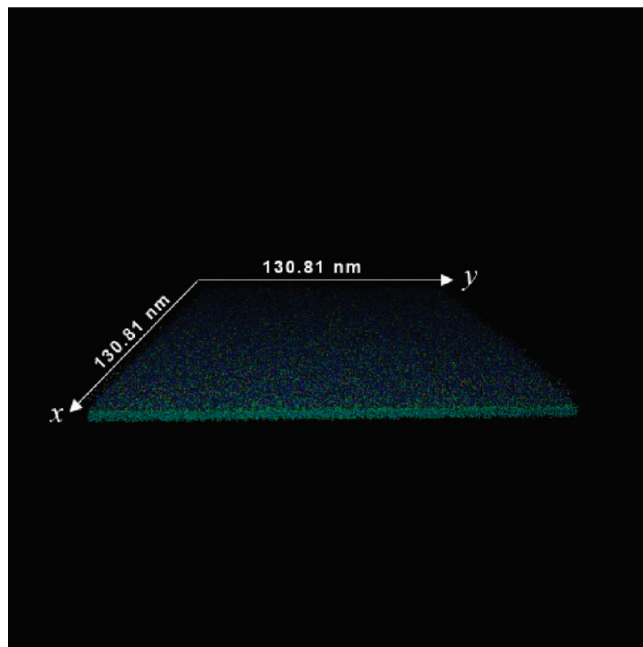


Figure 16. Snapshot of a system composed of 53 248 DPPC and 409 600 water molecules obtained by a parallel simulation. The grid size l used in the simulation was 2.5σ , and the density update frequency was 300 time steps.

very similar for PP and PF simulations. Similar conclusions can be made by comparing density profiles of any pair of two other lipids considered here, except for DOPC and DSPC. In this case, both PP and PF density profiles are very similar.

The calculated values D_{HH} are reported in Table 6 together with the reference PP and experimental values. The values of D_{HH} calculated from PF simulations are in good agreement with both PP simulations and experimental data. We want to stress that experimental values of D_{HH} lie in a very narrow range going from the smallest value of 3.6 nm for DPPC to the largest one of 4.0 nm for DSPC, and good reproduction of these values can be proof of the transferability of the chosen PF model. As previously discussed, DSPC and DOPC give very similar density profiles with both PP and PF models. This leads to the calculation of the same values of $D_{HH} = 4.1$ nm for these two lipids using PP models. Using PF models, according to the experimental trend, a larger value is obtained for the D_{HH} of DSPC (4.4 nm) and a smaller one for DOPC (4.0 nm).

In Figure 15, the total electron density profiles obtained by Kučerka et al. from X-ray scattering data for DOPC⁵³ and DMPC,⁵⁴ the ones obtained from PP and PF simulations, are plotted. In particular, the behavior of electron density of DOPC and DMPC is compared. As already found for DPPC (see Figure 3), the behavior of the calculated density profiles is smoother than the experimental ones. Furthermore, for DOPC, the position of the maximum of electron density profile of both PP and PF is shifted of about 0.5 nm. This is consistent with an overestimation of the D_{HH} (4.1 and 4.0 nm for PP and PF, respectively) with respect to the experimental value of 3.6–3.7 nm. For DMPC, the position of the maximum of the electron density profile of both PP and PF simulations is similar to the experimental one. In this case, the experimental value of D_{HH} is well reproduced (see Table 6).

CONCLUSIONS

Specific CG models for phospholipids and water suitable for hybrid particle field molecular dynamics simulations have been developed. These models and the set of parameters needed to evaluate interactions of particles with density fields are optimized to reproduce structural properties of reference PP simulations of DPPC. These parameters are transferable also to other phospholipids. The correct reproduction of the structural properties of the reference system depends on the density coarse-graining parameters. As expected, due to the smoothness of the PF interactions, the dynamics is faster in PF simulations. In particular, the ratio between diffusion coefficients calculated from PP and PF simulations goes from 3 to 7 depending on the degree of coarse-graining of the density field.

The computational efficiency of the PF approach allows one to accelerate the serial simulations by a factor of up to 10 for the considered systems. Furthermore, the peculiar formulation of the hybrid PF approach allows us a very efficient parallelization. To have an idea about the efficiency for the systems considered in this paper, 1 million steps of a simulation of a lipid bilayer system containing more than 1 million particles (a snapshot of this system containing a total of 1,048,576 particles is depicted in Figure 16) takes about 5 h on 96 processors (Intel E7330, 2.40 GHz).

In conclusion, the development of specific coarse-grained models suitable for hybrid PF simulation opens the way toward the simulation of large-scale systems employing models with chemical specificity.

ASSOCIATED CONTENT

S Supporting Information. Table with bond and angle parameters, plots with histograms of the radius of gyration and the angle between tails for DPPC. This information is available free of charge via the Internet at <http://pubs.acs.org>

AUTHOR INFORMATION

Corresponding Author

*E-mail: gmilano@unisa.it.

ACKNOWLEDGMENT

G.M. thanks MIUR (PRIN2008 and FIRB “RETE ITALNANONET”) for financial support and the HPC team of Enea (www.enea.it) for using the ENEA-GRID and the HPC facilities CRESCO (www.cresco.enea.it) in Portici, Italy. D.R. and G.M. thank Deutschen Forschungsgemeinschaft (DFG) for funding in the framework of the project “The study of detailed mechanism of polymers/biological membrane interactions using computer simulation” (RO 3571/3-1). T.K. thanks the Grant-in-Aid for Science from the Ministry of Education, Culture, Sports, Science and Technology, Japan.

REFERENCES

- (1) Venturoli, M.; Sperotto, M. M.; Kranenburg, M.; Smit, B. *Phys. Rep., Rev. Sect. Phys. Lett.* **2006**, 437 (1–2), 1–54.
- (2) Marrink, S. J.; de Vries, A. H.; Tieleman, D. P. *Biochim. Biophys. Acta, Biomembr.* **2009**, 1788 (1), 149–168.
- (3) Gurtovenko, A. A.; Anwar, J.; Vattulainen, I. *Chem. Rev.* **2010**, 110 (10), 6077–6103.
- (4) Psachoulia, E.; Marshall, D. P.; Sansom, M. S. P. *Acc. Chem. Res.* **2010**, 43 (3), 388–396.

- (5) Lyubartsev, A. P.; Rabinovich, A. L. *Soft Matter* **2011**, *7* (1), 25–39.
- (6) Bandyopadhyay, S.; Tarek, M.; Klein, M. L. *J. Phys. Chem. B* **1999**, *103* (46), 10075–10080.
- (7) Saiz, L.; Klein, M. L. *Acc. Chem. Res.* **2002**, *35* (6), 482–489.
- (8) Faller, R.; Marrink, S.-J. *Langmuir* **2004**, *20* (18), 7686–7693.
- (9) Pal, S.; Milano, G.; Roccatano, D. *J. Phys. Chem. B* **2006**, *110* (51), 26170–26179.
- (10) Bennett, W. F. D.; MacCallum, J. L.; Hinner, M. J.; Marrink, S. J.; Tieleman, D. P. *J. Am. Chem. Soc.* **2009**, *131* (35), 12714–12720.
- (11) Brannigan, G.; Lin, L. C. L.; Brown, F. L. H. *Eur. Biophys. J.* **2006**, *35* (2), 104–124.
- (12) Müller-Plathe, F. *Chemphyschem* **2002**, *3* (9), 754–769.
- (13) Peter, C.; Kremer, K. *Soft Matter* **2009**, *5* (22), 4357–4366.
- (14) Müller, M.; Katsov, K.; Schick, M. *Phys. Rep.* **2006**, *434* (5–6), 113–176.
- (15) Sintes, T.; Baumgaertner, A. *J. Phys. Chem. B* **1998**, *102* (36), 7050–7057.
- (16) Sintes, T.; Baumgartner, A. *Biophys. J.* **1997**, *73* (5), 2251–2259.
- (17) Lenz, O.; Schmid, F. *J. Mol. Liq.* **2005**, *117* (1–3), 147–152.
- (18) Goetz, R.; Lipowsky, R. *J. Chem. Phys.* **1998**, *108* (17), 7397–7409.
- (19) Marrink, S. J.; de Vries, A. H.; Mark, A. E. *J. Phys. Chem. B* **2003**, *108* (2), 750–760.
- (20) Marrink, S. J.; Mark, A. E. *J. Am. Chem. Soc.* **2003**, *125* (49), 15233–15242.
- (21) Marrink, S.-J.; Mark, A. E. *Biophys. J.* **2004**, *87* (6), 3894–3900.
- (22) Monticelli, L.; Kandasamy, S. K.; Periole, X.; Larson, R. G.; Tieleman, D. P.; Marrink, S.-J. *J. Chem. Theory Comput.* **2008**, *4* (5), 819–834.
- (23) Kawakatsu, T. *Statistical Physics of Polymers*; Springer: Berlin, 2004.
- (24) Matsen, M. W.; Schick, M. *Phys. Rev. Lett.* **1994**, *72* (16), 2660–2663.
- (25) Drolet, F.; Fredrickson, G. H. *Phys. Rev. Lett.* **1999**, *83* (21), 4317–4320.
- (26) Fredrickson, G. H.; Ganesan, V.; Drolet, F. *Macromolecules* **2002**, *35* (1), 16–39.
- (27) Lauw, Y.; Leermakers, F. A. M.; Stuart, M. A. C. *J. Phys. Chem. B* **2006**, *110* (1), 465–477.
- (28) Ly, D. Q.; Honda, T.; Kawakatsu, T.; Zvelindovsky, A. V. *Macromolecules* **2008**, *41* (12), 4501–4505.
- (29) Pinfield, V. J.; Horne, D. S.; Leermakers, F. A. M. *J. Chem. Soc., Faraday Trans.* **1997**, *93* (9), 1785–1790.
- (30) Balazs, A. C.; Singh, C.; Zhulina, E. *Macromolecules* **1998**, *31* (23), 8370–8381.
- (31) Roan, J. R.; Kawakatsu, T. *J. Chem. Phys.* **2002**, *116* (16), 7283–7294.
- (32) Roan, J. R.; Kawakatsu, T. *J. Chem. Phys.* **2002**, *116* (16), 7295–7310.
- (33) Marcelja, S. *Nature* **1973**, *241* (5390), 451–453.
- (34) Leermakers, F. A. M.; Scheutjens, J. *J. Chem. Phys.* **1988**, *89* (5), 3264–3274.
- (35) Leermakers, F. A. M.; Rabinovich, A. L.; Balabaev, N. K. *Phys. Rev. E* **2003**, *67* (1), 011910.
- (36) Muller, M.; Schick, M. *Phys. Rev. E* **1998**, *57* (6), 6973.
- (37) Szleifer, I.; Carignano, M. A. *Tethered Polymer Layers*. In *Adv. Chem. Phys.*; John Wiley & Sons, Inc.: New York, 2007; pp 165–260.
- (38) Muller, M.; Smith, G. D. *J. Polym. Sci., Part B: Polym. Phys.* **2005**, *43* (8), 934–958.
- (39) Daoulas, K. C.; Muller, M.; Stoykovich, M. P.; Park, S. M.; Papakonstantopoulos, Y. J.; de Pablo, J. J.; Nealey, P. F.; Solak, H. H. *Phys. Rev. Lett.* **2006**, *96* (3).
- (40) Detcheverry, F. A.; Kang, H. M.; Daoulas, K. C.; Muller, M.; Nealey, P. F.; de Pablo, J. J. *Macromolecules* **2008**, *41* (13), 4989–5001.
- (41) Milano, G.; Kawakatsu, T. *J. Chem. Phys.* **2009**, *130* (21), 214106.
- (42) Milano, G.; Kawakatsu, T. *J. Chem. Phys.* **2010**, *133*, 21.
- (43) Lindahl, E.; Hess, B.; van der Spoel, D. *J. Mol. Model.* **2001**, *7* (8), 306–317.
- (44) Marrink, S.-J.; Risselada, H. J.; Yefimov, S.; Tieleman, D. P.; de Vries, A. H. *J. Phys. Chem. B* **2007**, *111* (27), 7812–7824.
- (45) Nagle, J. F.; Zhang, R.; Tristram-Nagle, S.; Sun, W.; Petrache, H. I.; Suter, R. M. *Biophys. J.* **1996**, *70* (3), 1419–1431.
- (46) Kucherka, N.; Tristram-Nagle, S.; Nagle, J. F. *Biophys. J.* **2006**, *90* (11), L83–L85.
- (47) Milano, G. *OCCAM 3.0*; In University of Salerno: Salerno, Italy, 2007.
- (48) Katsaras, J.; Tristram-Nagle, S.; Liu, Y.; Headrick, R. L.; Fontes, E.; Mason, P. C.; Nagle, J. F. *Biophys. J.* **2000**, *78* (1), 116.
- (49) Tschöp, W.; Kremer, K.; Hahn, O.; Batoulis, J.; Bürger, T. *Acta Polym.* **1998**, *49* (2–3), 75–79.
- (50) Santangelo, G.; Di Matteo, A.; Müller-Plathe, F.; Milano, G. *J. Phys. Chem. B* **2007**, *111* (11), 2765–2773.
- (51) Carbone, P.; Karimi-Varzaneh, H. A.; Müller-Plathe, F. *Faraday Discuss.* **2010**, *144*, 25–42. 93–110. 467–81.
- (52) Balgavi, P.; Dubniková, M.; Kuerka, N.; Kiselev, M.; Yaradaikin, S.; Uhríková, D. *Biochim. Biophys. Acta, Biomembr.* **2001**, *1512* (1), 40–52.
- (53) Kucherka, N.; Nagle, J. F.; Sachs, J. N.; Feller, S. E.; Pencer, J.; Jackson, A.; Katsaras, J. *Biophys. J.* **2008**, *95* (5), 2356–2367.
- (54) Kucherka, N.; Liu, Y.; Chu, N.; Petrache, H. I.; Tristram-Nagle, S.; Nagle, J. F. *Biophys. J.* **2005**, *88* (4), 2626–2637.